We are IntechOpen, the world's leading publisher of Open Access books Built by scientists, for scientists

4,800
Open access books available

122,000
International authors and editors

135M
Downloads

Our authors are among the

154
Countries delivered to

TOP 1%
most cited scientists

12.2%
Contributors from top 500 universities

CLARIVATE ANALYTICS BOOK CITATION INDEX INDEXED

WEB OF SCIENCE™

Selection of our books indexed in the Book Citation Index in Web of Science™ Core Collection (BKCI)

Interested in publishing with us?
Contact book.department@intechopen.com

Numbers displayed above are based on latest data collected.
For more information visit www.intechopen.com

8

An Approximate Riemann Solver for Euler Equations

Oscar Falcinelli[1], Sergio Elaskar[1,2],
José Tamagno[1] and Jorge Colman Lerner[3]
[1]*Aeronautical Department, FCEFyN,*
Nacional University of Cordoba
[2]*CONICET*
[3]*Aeronautical Department, Engineering Faculty,*
Nacional University of La Plata
Argentina

1. Introduction

A fundamental subject leading to numerical simulations of Euler equations by the Finite Volume (FV) method, is the calculation of numerical fluxes at cells interfaces. The degree of accuracy of the FV numerical scheme, its ability to capture discontinuities and the correct prediction of the velocity of propagating waves, are all flow properties strongly dependent on the evaluation of numerical fluxes.

In many numerical schemes, the fluxes between cells are computed using truncated series expansions which based only on numerical considerations. These considerations to be strictly valid, must account for some degree of continuity in the functions and in their derivatives, but clearly, these continuity conditions are not satisfied when discontinuous solutions as shock waves or contact surfaces are present in the flow. This type of flow problems nevertheless, were solved with relative success until 1959. In that year Godunov published his work "A finite difference method for the computation of discontinuous solutions of the equations of Fluid Dynamics" (Godunov, 1959) in which an alternative approach for solving the system of Euler equations is presented. This new approach, in striking difference to previous ones, is basically supported by physical considerations and the essential part of it is the so called Riemann solver.

The excellent results obtained with the Godunov technique, prompted several researches to develop new FV numerical schemes for two and three dimensional applications, achieving second order accuracy and total variation diminishing (TVD) properties (Toro, 2009; LeVeque, 2004; Yee, 1989). These new schemes were built around the use of Riemann solvers, making them generally very accurate but computationally expensive. Such high computational cost is attributed to the iterative technique required to solve the system of five nonlinear algebraic equations needed to find, in all cells, an exact solution of the Riemann problem. Alternative schemes computationally less demanding, although less accurate and less robust, were then built based on approximate solutions of the Riemann problem (Toro, 2009).

In this article, a new non-iterative way of solving the full Riemann problem, applicable to three-dimensional and time dependent Euler equations, is presented. This non-iterative solution requires at the beginning of the computation and only once, the generation in situ of tabulated exact Riemann solutions from which the information needed can be retrieved using multiple-linear interpolation. To reduce the time to access during successive calculations, the original five independent variables of the exact Riemann problem are, by way of dimensional analysis, reduced to only three thus allowing the build-up of an easiest to handle data-based matrix with three degrees of freedom.

2. Description of the proposed Riemann Solver

Compressible and inviscid flow problems are governed by the Euler equations. In one dimension (1D), these equations can be written as:

$$U_t + F(U)_x = 0 \tag{1}$$

$$U = \begin{bmatrix} \rho \\ \rho u \\ E \end{bmatrix}; \quad F(U) = \begin{bmatrix} \rho u \\ \rho u^2 + p \\ (E+p)u \end{bmatrix} \tag{2}$$

U is the vector of conservative variables, F the vector of convective flows, t and x are the temporal and spatial coordinates respectively, ρ is the density, u the velocity in the x direction, p the pressure and E the total energy per unit volume. The subscript means differentiation with respect to time and space.

The Riemann problem solves de Euler equations in a 1D domain where initial conditions are given by two different constant states separated by a discontinuity. The solution of this 1D Riemann problem depends directly on the ratio x/t, and it will consist of three types of waves: two nonlinear, shock or expansion fan, and one linearly degenerate, the contact discontinuity. These waves are separating four constant states where the conservative vector U acquires from the left to the right the following values, U_L, U_{L^*}, U_{R^*} and U_R. The subscripts "L" and "R" indicate left and right, respectively, and the symbol "*" identify points located in the state between the nonlinear waves (star region).

To obtain the flow variations produced by the waves, the Riemann invariants technique for expansion and contact waves and of the Rankine-Hugoniot relationship for shock waves, must be implemented. In the Riemann problem, this generally leads to an algebraic system of nine equations with nine unknowns. The unknowns are the velocities of the three waves plus six variables necessary to characterize the states U_{L^*}, U_{R^*}. However, an analysis of the eigenstructure of the Euler equations allows to establish that both pressure p_* and particle velocity u_* between the left and right waves are constant, while the density take the two constant values ρ_{*L} and ρ_{*R} (Toro, 2009). Based on these considerations and after some algebraic calculations, the two equations listed below are obtained and used for solving the Riemann problem.

$$f_L(p_*, U_L) + f_R(p_*, U_R) + \Delta u = 0 \tag{3a}$$

$$u^* = \frac{1}{2}\left(u_L + u_R\right) + \frac{1}{2}\left[f_R\left(p_*, U_R\right) - f_L\left(p_*, U_L\right)\right] \tag{3b}$$

where $\Delta u = u_R - u_L$. Once Eq.(3a) is solved for p_* the solution for u_* is obtained from Eq.(3b) and the remaining unknowns are found by means of standard gas dynamic relations. The functions f_L and f_R represent relations across the left non-linear wave and across the right non-linear wave respectively, and are given by

$$f_K\left(p_*, U_K\right) = \left(p_* - p_K\right) \cdot \sqrt{\frac{A_K}{p_* + B_K}} \qquad if \qquad p_* \geq p_K \tag{4a}$$

$$f_K\left(p_*, U_K\right) = \frac{2 \cdot a_K}{\gamma - 1} \cdot \left[\left(\frac{p_*}{p_K}\right)^{\frac{\gamma-1}{2\cdot\gamma}} - 1\right] \qquad if \qquad p_* < p_K \tag{4b}$$

$$A_K = \frac{2}{(\gamma+1)\cdot\rho_K} \quad B_K = \frac{(\gamma-1)}{(\gamma+1)} \cdot p_K \tag{5}$$

where γ is the ratio of specific heats, K may be L or R depending on if the flow changes are evaluated across the nonlinear left or right waves, and a_K is the speed of sound in the left or right states. The Eq.(3a) is an implicit algebraic nonlinear equation on the only unknown p_*, and it must be solved using an iterative scheme. Once the pressure in the star region has been obtained, it is possible to calculate by means of explicit expressions the velocity u_* and the density at each side of the contact discontinuity.

In Eq.(3a), neither u_L nor u_R are explicitly written, but only its difference. Therefore the pressure in the star zone becomes only function of five variables:

$$p_* = f_1\left(\Delta u, \rho_L, p_L, \rho_R, p_R\right) \tag{6}$$

In this article, the dimensional analysis is used to reduce the number of independent variables necessaries for describing the gas-dynamics Riemann problem. From this point of view, it is possible to consider as reference variables the density and pressure from one side of the Riemann problem, for example, the right side.

$$\rho_{ref} = \rho_R \qquad p_{ref} = p_R \tag{7}$$

The Eq.(6) represents a relationship between pressures, velocities and densities. By means of the dimensional analysis, the densities can be written in non-dimensional form using a reference value such as ρ_R, the pressures using as reference p_R, and the velocities respect of $(\rho_R \; p_R)^{1/2}$. Then, the solution of a particular Riemann problem is determined by the following three parameters:

$$\pi_1 = \frac{\Delta u}{\sqrt{\frac{p_R}{\rho_R}}} \qquad \pi_2 = \frac{p_L}{p_R} \qquad \pi_3 = \frac{\rho_L}{\rho_R} \tag{8}$$

Different cases of Riemann problems with identical values of π_1, π_2, π_3 must have similar behavior, and the calculated relation p_*/p_R must have the same value for all cases. To ascertain this behavior for the non-dimensional approach proposed, several numerical examples are analyzed. Seven Riemann problems whose left and right conditions are indicated in the following table, and all of them satisfying the parameters π_1 = -0.78262, π_2 = 50, π_3 = 10, were tested:

ρ_L	u_L	p_L	ρ_R	u_R	p_R
1.2250E+00	1.0000E+02	1.0000E+05	1.2250E-01	0.0000E+00	2.0000E+03
4.9071E+01	8.4770E+02	8.7460E+06	4.9071E+00	6.9994E+02	1.7492E+05
6.7304E+00	6.5231E+02	1.0554E+07	6.7304E-01	2.1402E+02	2.1108E+05
4.1503E+00	7.8027E+02	1.1631E+07	4.1503E-01	1.9437E+02	2.3261E+05
9.4504E+00	6.4262E+02	1.5976E+07	9.4504E-01	1.8756E+02	3.1952E+05
3.0289E+01	2.9038E+02	2.9757E+06	3.0289E+00	1.8067E+02	5.9514E+04
3.6284E+01	3.0129E+02	6.5687E+05	3.6284E+00	2.5420E+02	1.3137E+04

Table 1. Test cases.

The relation p_*/p_R is obtained solving Eq.(3), and for the seven test cases considered it is found p_*/p_R = 13.312, which proves that the proposed non-dimensional analysis works properly. Then, it is possible to write the Eq.(3) only as function of π_1, π_2, π_3 and p_*/p_R.

Since in solving the Eq.(3) there are involved only three independent variables, a data-base matrix with three degrees of freedom containing the values of p_*/p_R for N values of π_1, M of π_2, and Q of π_3 is, in situ generated. Then, to find the solution of a particular Riemann problem, it is only necessary to calculate the corresponding values of π_1, π_2, π_3 and to interpolate for p_*/p_R in the N*x*M*x*Q matrix (from now, simply called A-matrix). Finally the pressure in the star zone can be calculated as:

$$p_* = \overline{\left(\frac{p_*}{p_R}\right)} \cdot p_R \tag{9}$$

where $\overline{\left(\frac{p_*}{p_R}\right)}$ is the interpolated value from the A-matrix. After calculating the pressure in the star region, the rest of the variables can be explicitly calculated using the same equations of the exact solver (Toro, 2009).

The previously described procedure involves the use of an interpolated value of pressure to calculate the density and velocity changes across each wave; however it is not the only possible procedure. Others alternatives are for instance, to develop arrangements with dimensionless density or dimensionless velocity variations across each wave.

To increase the approximate solution accuracy, it is desirable that the variation range of the parameters π_1, π_2, π_3 be as small as possible. One way is to reduce the range of π_2 or π_3 avoiding unneeded storage of data in symmetrical Riemann problems.

Two Riemann problems will be symmetric if the following conditions are satisfied:

$$\left(p_R\right)_A = \left(p_L\right)_B \qquad \left(\rho_R\right)_A = \left(\rho_L\right)_B \qquad \Delta u_A = \Delta u_B \tag{10}$$

Unnecessary storage in symmetrical cases can be avoided if it is adopted as the selection criterion of the reference variables (p_{ref} , ρ_{ref}) in Eq.(7), not the left or right pressure and density, but those of the higher pressure side. Thus, the reference state is the higher pressure initial state and the π_2 value will always be less than or equal to one.

To give a physical sense to the non-dimensional π_1 variable it is convenient to re-define it as:

$$\pi_1 = \frac{\Delta u}{\sqrt{\gamma \cdot \frac{p_{ref}}{\rho_{ref}}}} = \frac{\Delta u}{a_{ref}} \tag{11}$$

where a_{ref} is the sound velocity in the reference state and π_1 would be like a Mach number change between the left and right states in the Riemann problem. However π_1 is not strictly a change of the Mach number because a_{ref} is not the sound velocity neither that of the left state or that of the right.

Finally, it is clear that no interpolation is necessary when the solution of the Riemann problem possesses left and right expansion waves, because in this case the Eq.(3) can be solved analytically.

3. Comparison with other Riemann Solvers

To analyze the accuracy and computational efficiency of the proposed Riemann solver, comparisons with others solvers available in the literature (Toro, 2009), are made. Three were selected: one that, iteratively searches for the exact solution of Eq.(3), and others two, that they try to solve the Riemann problem with approximate schemes. To build-up the comparison, Riemann problems were generated randomly with values of the parameters π_1, π_2 and π_3 ranging between the limits set below:

$$-10.05 \le \pi_1 \le 4.95 \quad 0.05 \le \pi_2 \le 1 \quad 0.05 \le \pi_3 \le 5.05 \tag{12}$$

The following sub-sections explain how each one of the solvers selected for comparison works.

3.1 Iterative Riemann Solver

This solver searches by means of an iterative process the solution of Eq.(3a). This equation for any value of p shall be written as:

$$f_L\left(p, U_L\right) + f_R\left(p, U_R\right) + \Delta u = R\left(p\right) \tag{13}$$

where $R(p)$ is the residual to cancel; f_L and f_R, are calculated according to Eqs.(4 and 5).

Usually to iteratively solve Eq.(13), the Newton-Raphson method is implemented. This method requires the calculations of the function as well as of its derivative, which should

increase the computational cost of the method, but this increase is not significant because the evaluation of the derivative demands simple computations once the function has been evaluated. Since the derivative of the residual function, Eq.(13), is calculated by means of the functions f_L and f_R without considering U_R and U_L that are constant, it can then be written as:

$$\frac{d\left[f_L(p,U_L)\right]}{dp}+\frac{d\left[f_R(p,U_R)\right]}{dp}=\frac{d\left[R(p)\right]}{dp} \tag{14}$$

The derivatives $\frac{d\left[f_L(p,U_L)\right]}{dp}=f_L^{'}$ y $\frac{d\left[f_R(p,U_R)\right]}{dp}=f_R^{'}$ are calculated as:

$$f_K^{'}=\begin{cases}\sqrt{\frac{A_K}{B_K+p}}\cdot\left(1-\frac{p-p_K}{2\cdot\left(B_K+p\right)}\right) & \text{if} \quad p\geq p_K \\ \\ \frac{1}{\rho_K\cdot a_K}\cdot\left(\frac{p}{p_K}\right)^{\frac{-(\gamma+1)}{2\cdot\gamma}} & \text{if} \quad p<p_K\end{cases} \tag{15}$$

From the computational point of view it is noted that the most expensive steps involved in the numerical evaluation of Eq.(15) are the powers with fractional exponents. However, Eqs.(4a and 4b) and Eq.(15) show that these computational steps have already been made when the residual $R(p)$ is computed, and as a result of this its derivative calculation is relatively fast.

The Newton-Raphson algorithm applied to Eq.(13) can be written as:

$$p_{i+1}=p_i-\frac{R_{(p_i)}}{R_{(p_i)}^{'}} \tag{16}$$

where p_i and p_{i+1} are the pressure for the iteration i and i+1 respectively, R and R' are the residual function and its derivative.

In solving iteratively Eq.(13) difficulties may appears because, as Eq.(16) suggests, the pressure can becomes negative. To avoid this problem, the residual function is evaluated (considering $p = p_{min}$ and $p = p_{max}$, where $p_{min} = min[p_L,p_R]$ and $p_{max} = max[p_L,p_R]$. If both residuals are positive, the pressure which cancels the residual is less than p_L and p_R, and the Riemann problem has an explicit solution consisting of two rarefaction waves. If the residual corresponding to the maximum pressure is greater than zero and the corresponding to minimum pressure is less than zero, the Riemann problem have as solutions a shock wave and a rarefaction fan, and it is adopted as a first iteration the value of the minimum pressure (which will undoubtedly be lower than the pressure to cancel the residual). When both residuals are negative, the Riemann problem has two shock waves and the sought pressure will be greater than both, so as first iteration the maximum pressure value is adopted.

Using the above described procedure, it is possible to know beforehand the kind of solution expected for the Riemann problem at each iterations, which allows an effective selection of

the function given by Eq.(4), and thus slightly shortening the time needed to reach the correct solution.

3.2 Two-Rarefaction Riemann Solver (TRRS)

A particular solution of the gas-dynamics Riemann problem is given when both non-linear waves are rarefaction waves. In this case the pressure in the star region can be obtained analytically.

$$\frac{2\cdot a_L}{\gamma-1}\cdot\left[\left(\frac{p_*}{p_L}\right)^{\frac{\gamma-1}{2\cdot\gamma}}-1\right]+\frac{2\cdot a_R}{\gamma-1}\cdot\left[\left(\frac{p_*}{p_R}\right)^{\frac{\gamma-1}{2\cdot\gamma}}-1\right]+\Delta u=0$$

$$\Downarrow \tag{17}$$

$$p_*=\left[\frac{a_L+a_R-\Delta u\cdot\frac{(\gamma-1)}{2}}{\frac{a_L}{p_L^{\left(\frac{\gamma-1}{2\cdot\gamma}\right)}}+\frac{a_R}{p_R^{\left(\frac{\gamma-1}{2\cdot\gamma}\right)}}}\right]^{\left(\frac{2\cdot\gamma}{\gamma-1}\right)}$$

When the pressure exceeds the value of $p_{\min}$, and the Eq.(4a) instead of Eq.(4b) to calculate the f_K functions is used, there are no discontinuities in the residual function and in its derivatives. This particular behavior of the Eq.(4a) and of its first derivative implies that the error incurred is at most of second order if instead of Eq.(4a), the Eq.(4b) is utilized.

However, if the Eq.(4b) is used to calculate the function f_K the ability to obtain analytically the value p_*, is lost. The TRRS method, suggests to calculate the pressure in the star region always using the Eq.(17), no matter what kind of Riemann problem is studied. The error of this method will be null for the Riemann problems with two rarefaction waves ($p_* \le p_{\min}$) and will increase as p_* becoming higher and moves away from $p_{\min}$.

3.3 Two-Shock Riemann solver (TSRS)

The TSRS is the opposite case of the TRRS. In the TSRS the solution of the Riemann problem is obtained considering that both non-linear waves are shocks. Then the functions f_K are given by the Eq.(4b) and the Eq.(3a) can be written as shown bellow:

$$(p_*-p_L)\cdot\sqrt{\frac{\frac{2}{(\gamma+1)\cdot\rho_L}}{p_*+\frac{(\gamma-1)}{(\gamma+1)}\cdot p_L}}+(p_*-p_R)\cdot\sqrt{\frac{\frac{2}{(\gamma+1)\cdot\rho_R}}{p_*+\frac{(\gamma-1)}{(\gamma+1)}\cdot p_R}}+\Delta u=0$$

$$\Downarrow \tag{18}$$

$$(p_*-p_L)\cdot g(p_*,U_L)+(p_*-p_R)\cdot g(p_*,U_R)+\Delta u=0$$

where

$$g(p,U_K)=\sqrt{\frac{\frac{2}{(\gamma+1)\cdot\rho_K}}{p+\frac{(\gamma-1)}{(\gamma+1)}\cdot p_K}} \tag{19}$$

The TSRS does not provide an analytical solution for p_*, and it is necessary an iterative process beginning with an approximation for p_* called p_0. p_0 is used to calculate the value of $g(p_0,U_L)$ and $g(p_0,U_R)$. Then, assuming $g(p_0,U_L)$ and $g(p_0,U_R)$ constants the Eq.(18) is lineal and it is possible to obtain p_* as:

$$p_*=\frac{p_L\cdot g(p_0,U_L)+p_R\cdot g(p_0,U_R)-\Delta u}{g(p_0,U_L)+g(p_0,U_R)} \tag{20}$$

Following the book (Toro, 2009) the approximation of p_* can be expressed as:

$$p_0=\frac{p_L+p_R}{2}+\frac{u_L+u_R}{2}\cdot\frac{\rho_L+\rho_R}{2}\cdot\frac{a_L+a_R}{2} \tag{21}$$

Although the TSRS scheme, even when applied to cases with two shock waves does not provide an exact solution, it is very robust and has become one of the more implemented approximated schemes to solve the Riemann problem.

3.4 Approximate and Adaptive Riemann solver using the TSRS and TRRS

The adaptive solver developed in this work is compared with an approximate Riemann solver that, as shown by Toro (2009), bind together the advantages of the TRRS and TSRS schemes. This Adaptive Riemann solver obtains the approximate p_0 as given by Eq.(21), then compare this pressure with p_{min} and p_{max} , and the pressure in the star region will be:

$$p_*=\begin{cases}p_{*TRRS} & \text{if } p_0\le p_{\min}\\ p_0 & \text{if } p_{\min}<p_0<p_{máx}\\ p_{*TSRS} & \text{if } p_0\ge p_{máx}\end{cases} \tag{22}$$

being p_{*TRRS} and p_{*TSRS} the pressures obtained using the TRRS and TSRS solvers respectively.

The comparatives results are presented in Section 5 of this chapter.

4. Description of the implemented schemes

In order to test the usefulness of the proposed Riemann solver, four computer codes were developed based on broadly well-known formulations. Three of them solve one dimensional problem applying second order accurates TVD schemes, and the other one applies a first order method to solve two dimensional problems. These formulations were selected because they require that a Riemann solver be implemented.

To compare the impact of the proposed Riemann solver in terms of accuracy as well as computational efficiency, all the numerical codes built have two versions, one of them works with the exact iterative solver and the other with the one here proposed.

The numerical schemes that the developed codes use are: the two-dimensional Godunov approach, the one-dimensional versions of the HLLC - Harten, Lax, van Leer Contact - (Toro, 2009), MUSCL - Monotonic Upstream-Centered Scheme for Conservation Laws - (van Leer, 1985 and Toro, 1994) and finally the RCM - Random Choice Method - method (Chorin, 1977).

The following sub-sections explain each one of them.

4.1 One-dimensional HLLC TVD method

Consider Figure 1, were the complete structure of the solution of the Riemann problem in terms of the slowest S_L and fastest S_R waves, and a middle wave of speed S_* is contained. Note that the HLLC Riemann solver does not compute the speed of the waves, but in order to determine completely the numerical fluxes an algorithm for computing the wave speeds has to be provided.

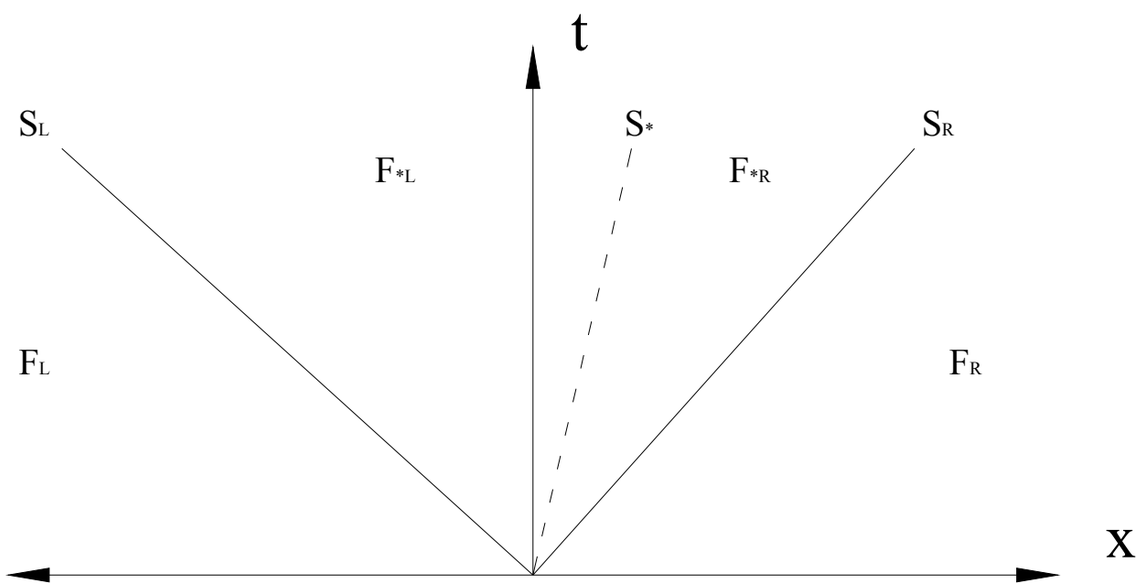

Fig. 1. Riemann problem for the HLLC method.

By applying Rankine-Hugoniot conditions across each of the waves S_L , S_* , S_R it can be obtained

$$R.H. \Rightarrow F_{*_L} - F_L = S_L \cdot \left(U_{*_L} - U_L\right) \tag{23a}$$

$$R.H. \Rightarrow F_{*_R} - F_{*_L} = S_* \cdot \left(U_{*_R} - U_{*_L}\right) \tag{23b}$$

$$R.H. \Rightarrow F_R - F_{*_R} = S_R \cdot \left(U_R - U_{*_R}\right) \tag{23c}$$

These are three equations for the four unknowns vectors U_{*L}, U_{*R}, F_{*L} and F_{*R}. The aim is to find the vectors U_{*L}, and U_{*R}, so that the fluxes F_{*L} and F_{*R} can be determined from Eq. (23).

From Eq.(23a) and Eq.(23c), F_L and F_R can be written as:

$$F_L = F_L + S_L \cdot (U_L - U_L) \tag{24}$$

$$F_R = F_R - S_R \cdot (U_R - U_R) \tag{25}$$

Introducing these last two expressions in Eq.(23b), it can be re-arranged as:

$$U_{*R} \cdot (S_R - S_*) + U_{*L} \cdot (S_* - S_L) = F_L - F_R + S_R \cdot U_R - S_L \cdot U_L \tag{26}$$

The Eq.(26) has three scalar equations and six unknowns, the components of U_{*L} and U_{*R}. The following new conditions are now imposed on the approximate Riemann solver

$$u_{*R} = u_{*L} = u_* \quad p_{*R} = p_{*L} = p_* \tag{27a}$$

which are satisfied by the exact solution. In addition, it is justified and convenient, to set

$$S_* = u_* \tag{27b}$$

that is, the star zone velocity must be equal to the contact discontinuity velocity.

Then, only one closure conditions remains to be set. In (Toro, 2009), the following is proposed:

$$\rho_{*K} = \rho_K \cdot \left(\frac{S_K - u_K}{S_K - S_*} \right) \tag{28}$$

Equation (27a) sets that the star zone velocity must be equal to the contact discontinuity velocity. To avoid confusion are called RHS1, RHS2 and RHS3 the first, second and third scalar components of the RHS vector of Eq.(26). It possible to show that to satisfy simultaneously the Eqs.(26 and 27):

$$S_* = \frac{RHS2}{RHS1} \tag{29}$$

$$p_* = \frac{RHS3 - \frac{S_*}{2} \cdot RHS2}{(S_R - S_L)} (\gamma - 1) \tag{30}$$

To obtain Eq.(30) was used the relation $E = \frac{\rho}{2} u^2 + \frac{p}{\gamma - 1}$.

The complete scheme shall consist on obtaining an estimation of S_L and S_R, on calculating S_* and p_* using Eqs.(29 and 30) respectively, and then determining ρ_{*R} and ρ_{*L} through Eq. (27). Finally the flow vectors F_{*L} and F_{*R} by means of the Eq. (24 and 25) are evaluated.

To estimate, either S_L or S_R when there is a rarefaction fan, it has been proposed to use the wave velocity in contact with the undisturbed state, and when there is a shock wave directly to use the shock velocity (Toro, 2009).

The difference between a first order, second order and TVD schemes are inherent to the structure of the numerical fluxes at cells interfaces. Calling wave-1, wave-2 and wave-3 those that separate the *L* and **L*, **L* and **R*, **R* and *R* states respectively; the algorithm in this paper implemented is

$$F_{i+1/2} = \frac{1}{2}\left(F_i + F_{i+1}\right) - \frac{1}{2}\sum_{j=1}^{3} sign\left(S_j\right)\phi_{i+1/2}^{j}\,\Delta F_{i+1/2}^{j} \tag{31}$$

being *i* and *i*+1 the left and right cells and $\phi_{i+1/2}^{j}$ is the limiter function for the wave-*j*. In this work are shown only the results obtained using a Van Leer limiter function; however the scheme works efficiently with other limiters.

Finally, the flow state vector is actualized at each time step by means of the explicit scheme:

$$U_i^{n+1} = U_i^{n+1} + \frac{\Delta t}{\Delta x}\left(F_{i-1/2} - F_{i+1/2}\right) \tag{32}$$

4.2 MUSCL TVD one-dimensional method

To construct discrete second-order accurate schemes the MUSCL method proposed by Hancock (van Leer, 1985) carries out the following steps:

Step 1. Choice of a suitably slope vector Δ_i and data reconstruction with boundary interpolated values.

Step 2. For each cell the boundary extrapolated values are evolved by a half time interval

Step 3. Solve the Riemann problem with data provided after Step 2.

Step 4. Compute new inter-cell fluxes and state vectors to complete one time interval

In the first step, using the flow solution from the previous time and applying some particular criterion, determine the slope on each cell, as shown in Figure 2.

Next, considering the slope in each cell, the state vector or independent state variables are extrapolated from the cell center to the cell boundary, namely

$$U_i^L = U_i - \frac{\Delta_i}{2} \quad U_i^R = U_i + \frac{\Delta_i}{2} \tag{33}$$

In the second step, it is calculated the evolution of states variables by a time ½ Δt (Fig. 3) according to:

$$\Delta_i^{\frac{\Delta t}{2}} = \frac{\Delta t}{2\cdot\Delta x}\cdot\left[F\left(U_i^L\right) - F\left(U_i^R\right)\right] \tag{34}$$

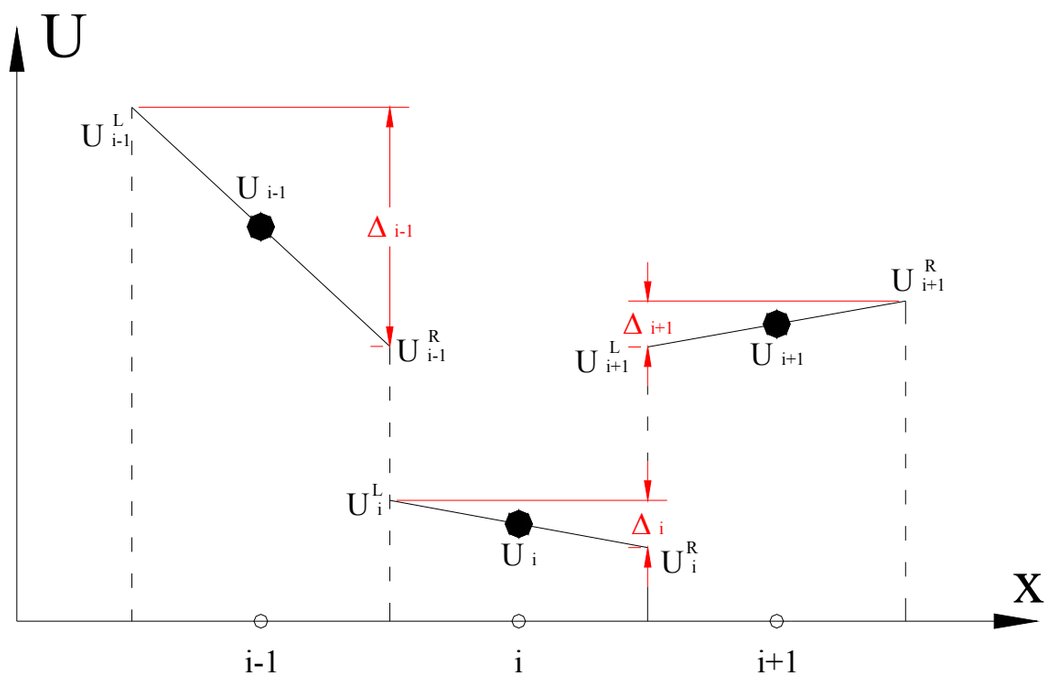

Fig. 2. MUSCL method data reconstruction.

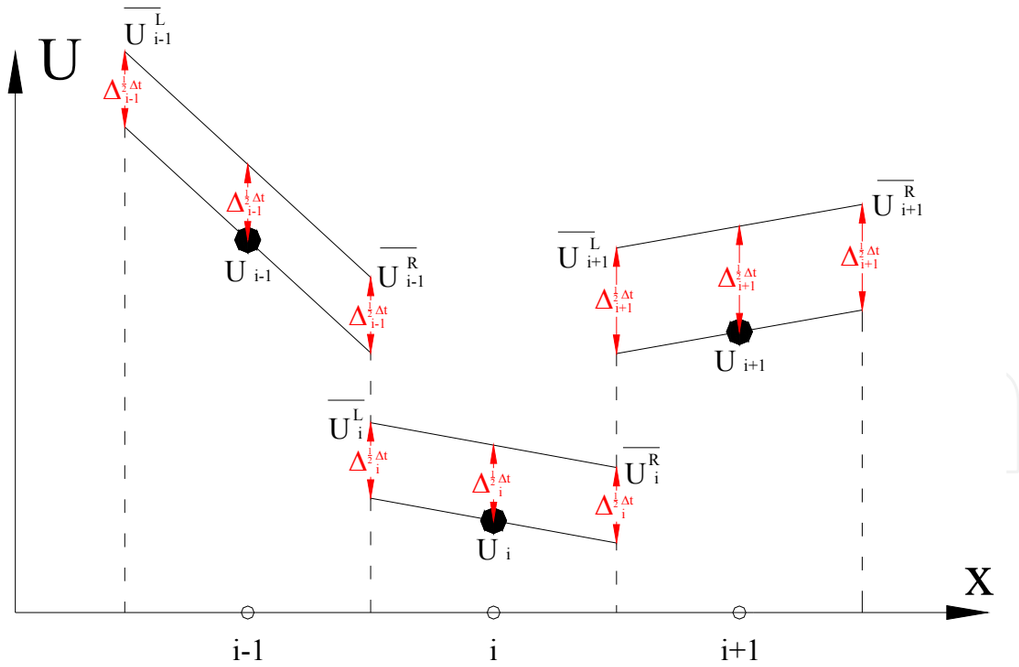

Fig. 3. Half time evolution in the MUSCL method.

Notice, that after using Eq.(34) the discontinuities between cells are actualized, and the Riemann problems are calculated using the half time evolved state vectors. Thus, at the i+½ interface the right adjacent initial state for the Riemann problem is given by

$$\overline{U_i^R} = U_i^R + \Delta_i^{\Delta t/2} = U_i + \frac{\Delta_i}{2} + \frac{\Delta t}{2\Delta x} \cdot \left[F\left(U_i^L\right) - F\left(U_i^R\right) \right] \tag{35}$$

and the left state by

$$\overline{U_{i+1}^L} = U_{i+1}^L + \Delta_{i+1}^{\Delta t/2} = U_{i+1} - \frac{\Delta_{i+1}}{2} + \frac{\Delta t}{2\Delta x} \cdot \left[F\left(U_{i+1}^L\right) - F\left(U_{i+1}^R\right) \right] \tag{36}$$

Once solved the Riemann problems the new inter-cell fluxes and state vectors are calculated for the complete time step (step four).

In this chapter, the following criterion to evaluate the slopes at the cells is used (Toro, 2009).

$$\Delta_i = \begin{cases} \max\left[0, \min\left(\beta\Delta_{i-1/2}, \Delta_{i+1/2}\right), \min\left(\Delta_{i-1/2}, \beta\Delta_{\Delta_{i+1/2}}\right)\right] & \text{si } \Delta_{\Delta_{i+1/2}} > 0 \\ \min\left[0, \max\left(\beta\Delta_{i-1/2}, \Delta_{\Delta_{i+1/2}}\right), \max\left(\Delta_{i-1/2}, \beta\Delta_{\Delta_{i+1/2}}\right)\right] & \text{si } \Delta_{\Delta_{i+1/2}} \leq 0 \end{cases} \tag{37}$$

where:

$$\Delta_{i-1/2} = U_i - U_{i-1} \quad \Delta_{i+1/2} = U_{i+1} - U_i \tag{38}$$

and β is a variable specifying the limiter function. Using Eqs.(37 and 38) the MUSCL scheme becomes TVD.

The results presented in Section 5 has been obtained using the SUPERBEE limiter function ($\beta = 2$).

4.3 The TVD Random Choice Method (RCM)

The RCM method can be seen as a modification of the Godunov method (Chorin, 1977). In the Godunov method, at the beginning of each time step, the state vector or independent states variables are considered constant within each cell. This piece-wise constant distribution of data at each time level, define local Riemann problems at the interface between neighboring cells.

To advance to the next time level, the Godunov method utilizes an integral average of local solutions of Riemann problems. Then, new averaged state vectors for all the cells are calculated via integrals

$$U_i^{n+1} = \frac{\int_{-\Delta x/2}^{\Delta x/2} U_{(x)}\, \delta x}{\Delta x} \tag{39}$$

where $U_{(x)}$ is the state vector solution within the i-cell, which has been obtained as solution of two adjacent Riemann problems (right i+½ , and left i–½).

The RCM and Godunov methods are similar in the sense that both use the exact solution of the Riemann problem. However, the RCM, instead of averaging according to Eq.(39), advances to the next time level assigning to each cell a picked value $U_{(x)}$ of the state vector

contained in the local solution. The picked up state depends on a point x randomly chosen within the sampling range $-\Delta x/2$ and $\Delta x/2$.

The RCM main advantage stands in its capacity to capture discontinuities separating constant states. It does not introduce artificial dissipation, shock waves and contact discontinuities are solved with infinite definition: the complete jump is produced in only one cell, and this accuracy does not get lost during time evolution.

However, the scheme has some disadvantages:

- The scheme introduces discontinuities in zones with smooth variations.
- The discontinuity velocities are random variables, only their average is the correct velocity. Usually the discontinuity places are not determined correctly.
- The scheme it is not strictly conservative.
- The randomness is tolerable when solving homogeneous systems, i.e. no source terms.
- The RCM can not be applied to solve multidimensional non linear problems via splitting techniques.

4.4 Two-dimensional Godunov method

It is well known that the original scheme (Godunov, 1959) is only first order accurate, which make it unsuitable for application to practical problems. Well resolved simulations will require the use of very fine meshes with the associated computing cost. Therefore, the original scheme was modified by incorporating concepts related to integral formulation of the Euler equations. These concepts have allowed substantial increments of computing time intervals.

The theoretical foundations of updated Godunov schemes are based on characteristics of the Riemann problem solution. This solution depends on the ratio x/t, but it does not on time alone or position alone. At any cell interface ($x = 0$, for the local Riemann problem), the state vector remains constant until a coming wave from the neighbor cell reaches the interface. An integral analysis shows that the cell average state vector U can be calculated analytically using the flux vectors at the cell boundaries. However, it is necessary to solve two Riemann problems at the interfaces of the cell in question. The state vector change ΔU_i in the i-cell and during one time interval Δt can be evaluated as:

$$\Delta U_i = \frac{\Delta t}{\Delta x}\left[F\left(U_{x/t=0}^{i-1/2}\right) - F\left(U_{x/t=0}^{i+1/2}\right)\right] \tag{40}$$

were $F(U_{x/t=0})$ are the Godunov inter-cell numerical fluxes; and $U_{x/t=0}^{i-1/2}$ and $U_{x/t=0}^{i+1/2}$ are the similarity solutions evaluated at $x/t=0$ of the Riemann problems at the interface i–½ e i+½ respectively.

The fluid dynamics fundamentals of the Gudonov method applicable to two dimensional problems, are similar to those explained above. However to account for the physical two-dimensionality of non Cartesian geometries, some changes must be introduced. These are:

- The flux balance must be extended to all sides of two-dimensional cells
- To solve the Riemann problems, the direction of an outward unit vector normal to each side of multilateral shaped cell has to be determined.

Assuming that the local Riemann problems, in a system of coordinates aligned with the normal unit vector to each side of the cell have been solved, and the corresponding numerical fluxes have been obtained, then the alternative expression to Eq.(40) for non Cartesian geometries becomes

$$\Delta U_i = -\frac{\Delta t}{A}\sum_{j=1}^{k}\overline{F}\left(U_{x/t=0}^{i-1/2}\right)\bullet\overline{n_j}\Delta s_j \tag{41}$$

here k is the numbers of cell sides, and $\overline{F}$ the flux vector. $\overline{n_j}$ is the outward unit normal vector , $\bullet$ expresses the interior product and Δs_j is the side length.

5. Results

Results obtained using the approximate TRRS, TSRS and Adaptive RS, are in the next sub-section presented and compared with the new scheme proposed in this article. Comparison with results produced by HLLC, MUSCL and RC methods are presented, in the following after sub-section.

5.1 Results using approximate Riemann solvers

To analyze the behavior of the approximate solvers with randomly chosen values of the parameters π_i within the range given by Eq.(12), 10^6 cases of Riemann problems are studied. Of them, 65% were cases with two shock waves, 6% with one shock and one rarefaction wave and the remaining 29% with two rarefaction waves.

To systematized the analysis, in all Riemann problems the following initial conditions to the right state are established

$$\rho_R = 1\frac{Kg}{m^3} \qquad u_R = 0\frac{m}{s} \qquad p_R = 1\frac{N}{m^2} \tag{42}$$

The initial conditions for the left states are calculated using values of the parameters π_1, π_2 and π_3 picked-out from the intervals defined in Eq.(12) :

$$u_L = -\pi_1\cdot\sqrt{\gamma\cdot\frac{p_R}{\rho_R}} \qquad p_L = \pi_2\cdot p_R \qquad \rho_L = \pi_3\cdot\rho_R \tag{43}$$

To heighten the behavior of the approximate Riemann solvers, in the following table are listed the worst approximate test values for the TRRS, the TSRS, the adaptive RS and the new proposed scheme.

Solver	ρ_L	u_L	p_L	ρ_R	u_R	p_R	Solver prediction	Exact solution
TRRS	4.9733	11.8082	0.0507	1	0	1	998.7362	81.2775
TSRS	4.9182	11.8582	0.0564	1	0	1	31.8961	81.6784
Adaptive	4.9182	11.8582	0.0564	1	0	1	31.8961	81.6784
Proposed	0.0739	11.8752	0.9274	1	0	1	9.5344	9.6541

Table 2. Worst approximated solutions after solving Riemann test cases.

Note that for the three first solvers, the worst results appear when there are relatively strong shock waves. Also, it is noted that the most poorly test case predicted is the same for the TSRS and the Adaptive Riemann solvers. This is so because when the star pressure is highest that both initial pressures, the Adaptive solver uses the same calculation scheme that the TSRS.

The percent error for each tested Riemann solvers is:

TRRS	TSRS	Adaptive	New scheme
1128.80%	60.95%	60.95%	1.24%

Table 3. Percent error for Riemann solvers.

The CPU time used by each approximate solver given as a percentage of the necessary CPU time for the exact Riemann solver is:

TRRS	TSRS	Adaptive	New scheme
38.62%	25.93%	31.60%	34.57%

Table 4. Percent of CPU time.

It is probable that the comparison between Riemann solvers based only on worst test results may not be considered representative and in consequence objectionable. Therefore, another variable based on the average error of all the pressures computed in the star region for the approximate solvers, is introduced. The results (in N/m^2) are shown below:

TRRS	TSRS	Adaptive	New scheme
37.371	7.1504	7.0931	0.0019

Table 5. Average error.

Repeating the previous analysis, but adding the restriction that the exact pressure p^* in each case is bounded to $0.1\ p^L < p^* < 10\ p^L$ and $0.1\ p^R < p^* < 10\ p^R$, and in this manner avoiding the formation of high-intensity shocks and near-vacuum conditions, the worst computed cases for each solver are:

Solver	ρ_L	u_L	p_L	ρ_R	u_R	p_R	Solver prediction	Exact solution
TRRS	2.4112	4.2348	0.9999	1	0	1	12.5554	9.9950
TSRS	0.8759	5.3169	1.0013	1	0	1	6.7847	9.9618
Adaptive	0.8759	5.3169	1.0013	1	0	1	6.7847	9.9618
Proposed	0.0712	11.7759	0.9424	1	0	1	9.2260	9.3234

Table 6. Worst approximated solutions after solving Riemann test cases with restrictions in p^*.

The percent error for each of the tested Riemann solvers using a bounded p^* are:

TRRS	TSRS	Adaptive	New scheme
25.62%	31.89%	31.89%	1.05%

Table 7. Percent errors.

5.2 Results obtained using different numerical schemes

To compare the goodness and shortcoming of the HLLC, MUSCL, RCM and two-dimensional Godunov numerical schemes, an identical test case for all of them is implemented. The two-dimensional software inclusive, it is compared solving the same one dimensional test case.

The selected test case is a 2 meters length shock tube (and for the two-dimensional simulations $0.067m$ in height). The shock tube was selected because it is possible to reach an exact solution, and is a very popular benchmark for compressible computational fluid dynamics.

The shock tube has two sections of equal length separated by a diaphragm (discontinuity on the initial condition), and both sections are filled with air at the same temperature. Initially, the velocities along the tube are null. Inside the right section, the initials pressure and density are $p = 10^5 N/m^2$, $\rho = 1.225 kg/m^3$ respectively, and in the left section are $p = 10^4 N/m^2$, $\rho = 0.1225 kg/m^3$. For these initial conditions, the solution after the diaphragm is broken is known. It is composed by a shock wave traveling to the right at $543.4m/s$, and one contact surface also moving to the right at $277.6m/s$. There is also, a rarefaction fan traveling to the left, its wave tail is moving at $338.1m/s$ (the sound speed of the stagnant gas in the left section) and its front at $4.9m/s$.

The flow properties at the four states limited by the above described discontinuities and the continuous wave are:

	L	$*L$	$*R$	R
ρ	1.225	0.4995	0.2504	0.1225
u	0	277.6	277.6	0
p	100000	28482	28482	10000

Table 8. Shock tube states flow properties.

In all tests the mesh has 200 cells evenly distributed along the tube. In the two-dimensional simulations a structured mesh possessing 2400 triangles is used (see Figure 4)

Fig. 4. Mesh for two-dimensional simulations.

The obtained results are presented in Figures 5 to 8. In each figure there are three lines; one represents the exact solution (blue), another the solution using the exact Riemann solver

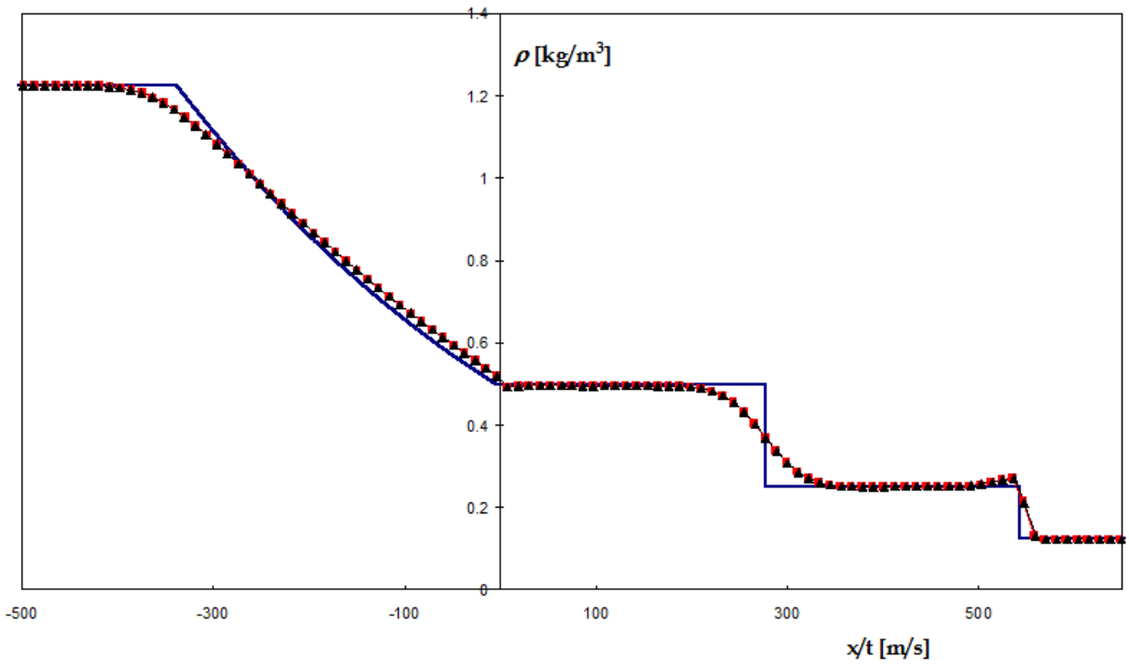

Fig. 5. Two-dimensional Godunov method. Blue line: theoretical solution. Red squares: exact solvers. Black triangles: approximate solver.

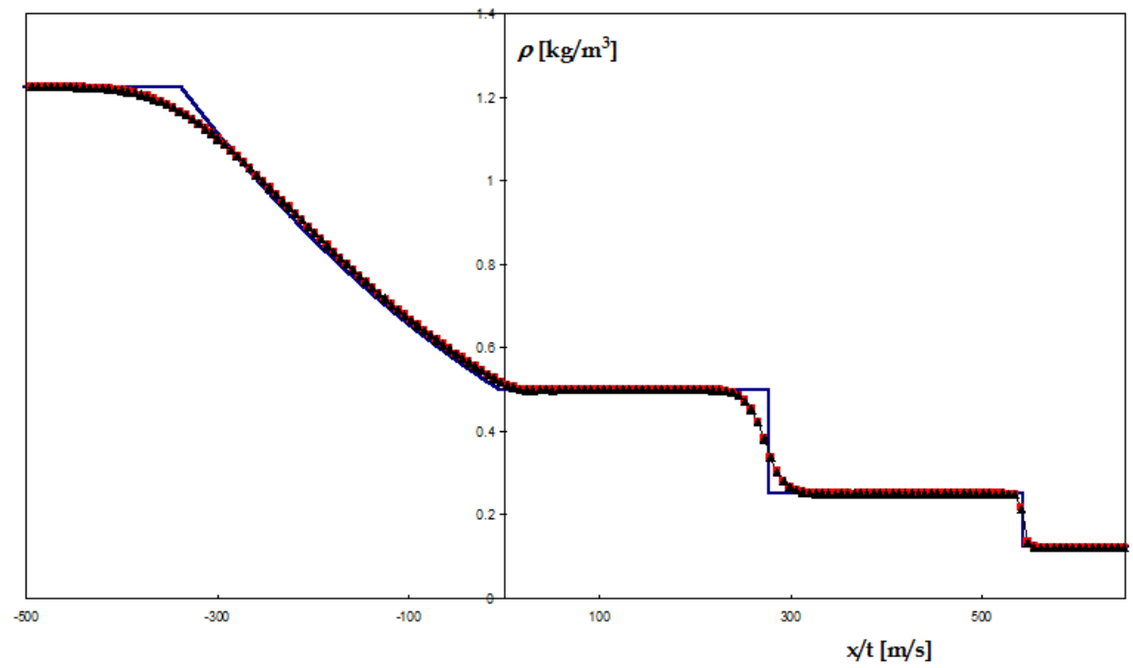

Fig. 6. One-dimensional HLLC method. Blue line: theoretical solution. Red squares: exact solvers. Black triangles: approximate solver

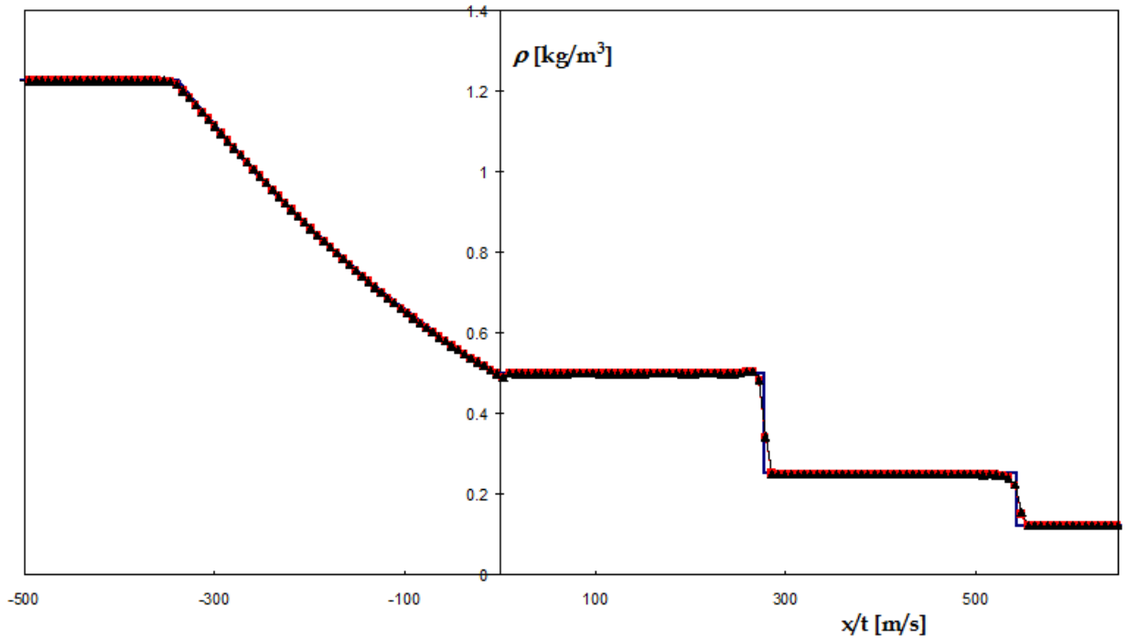

Fig. 7. One-dimensional MUSCL method. Blue line: theoretical solution. Red squares: exact solvers. Black triangles: approximate solver

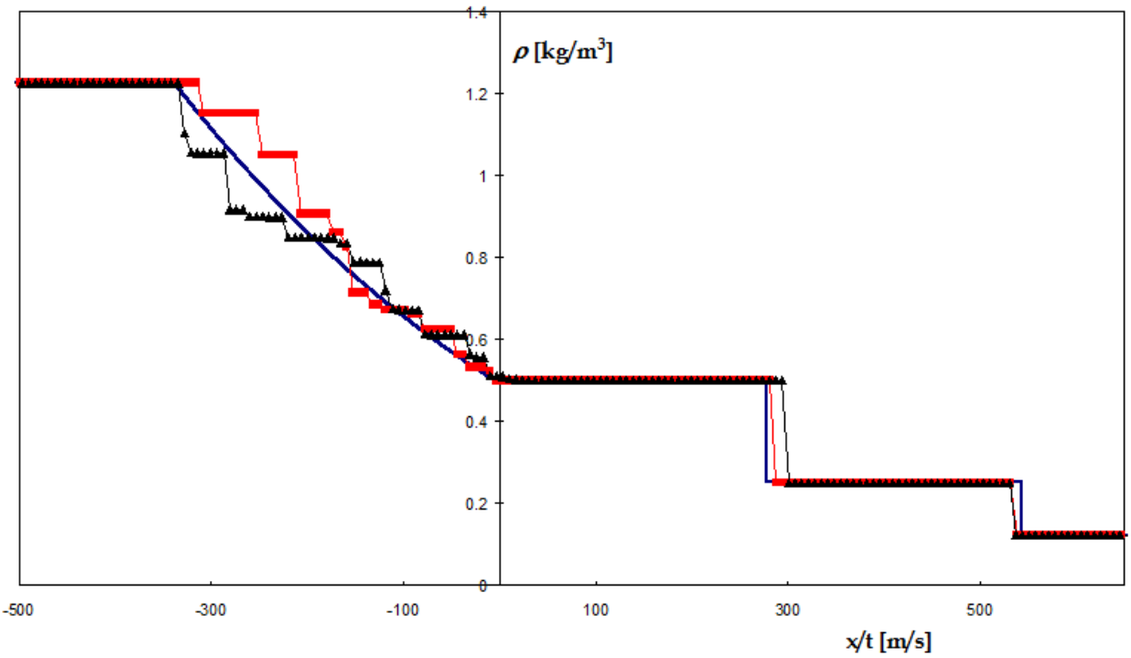

Fig. 8. One-dimensional RCM method. Blue line: theoretical solution. Red squares: exact solvers. Black triangles: approximate solver

(red with squares), and finally the third line shows the results obtained using the approximated Riemann solver proposed in this work (black with triangles). The two dimensional Godunov results shown are computed values along the tube center line.

From Figures 5 to 8 it can be deduced that the results calculated using, either the exact Riemann solver or the new proposed approximation, are practically identical, except for the RCM method. The differences between the numerical results presented in Figures 5 to 7 are less than 1%. For the RCM, the differences are greater; however it is believe that such differences are mainly due to the method randomness, and not to the Riemann solver itself.

In Figure 9 are plotted percentages of the computing time spent for each of the considered numerical schemes to complete a determined percent of the given task, either using the exact Riemann solver or the proposed approximation. Note that in Figure 9, the one hundred percent value has been assigned to all the results that the numerical schemes have produced using the new approximation in solving the Riemann Problem, while the other ones also plotted in percentages, are obtained through the same numerical schemes, but using now the exact Riemann solver.

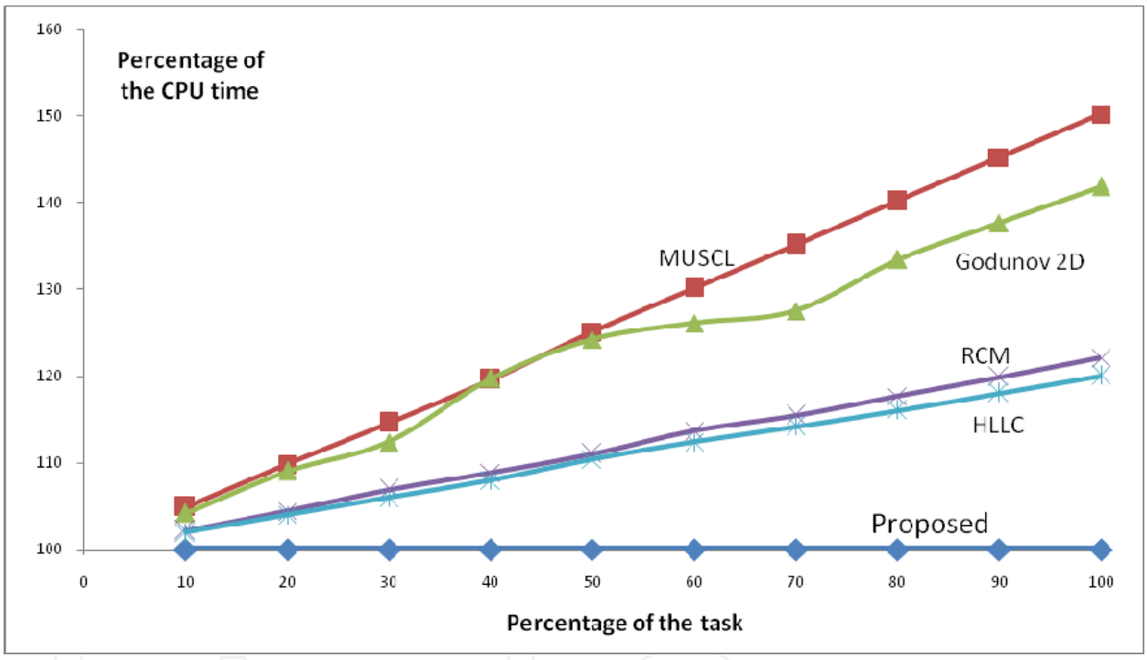

Fig. 9. CPU times evaluation.

It can be seen that using the proposed new approximate Riemann solver, less computing time is needed. In terms of CPU time, the percentages of savings achieved are listed bellow

GODUNOV 2D	HLLC	MUSCL	RCM
41.8%	20.0%	50.2%	22.1%

Table 9. Percent of CPU time.

6. Conclusions

After comparing the accuracy of the new proposed non iterative Riemann solver with the TRRS, the TSRS and the Adaptive RS, it has been found that for all pressure values computed in the star region, the average error of the new solver is notably smaller than

the average error of all the others approximated Riemann solvers (Table 5). In terms of the worst pressure values obtained in the star region (Table 2), the percentage error of the new solver is almost 50 time smaller than the best percentage obtained by the other solvers (Table 3). From the point of view of computational cost, it is higher if compared with the Adaptive solver and TSRS by 33.3 % and 9.4% respectively, but lower if the comparison is made with the TRRS. However, the new solver presented has a higher cost-benefit ratio.

It can be argued that the extremely high degree of uncertainty presented by the TRRS was due to the range of sampled Riemann problems (they mostly were problems with two shocks). However, in cases with well defined two rarefaction waves, the TRRS does not offer advantages over an exact Riemann solver because both perform the same operations.

Although the proposed solver has already shown to be efficient, it still requires a sequence of operations that others solvers do not need. For instance, before carrying out the interpolation on a data-base matrix of Riemann solutions, the matrix must be generated (a 100x100x100 matrix like the one used in this paper, requires the exact solution of 106 Riemann problems). However, this matrix is calculated only once at the beginning of the computation and it has only three degrees of freedom, which makes it of easy handling.

The numerical results obtained with HLLC, MUSCL and Godunov schemes, have shown that the new solver is accurate and robust, and no significant differences were found when results are compared with the exact Riemann solver. In addition, it shows appreciable advantages in terms of CPU time.

Modifications on the implementation of the new solver are suggested to benefits from the advantage of using the fully analytical solution in two expansion waves Riemann problems, and only the new approximate solver when there are Riemann problems with shock waves. Furthermore, it shall be desirable to redefine the parameter π_1 avoiding the square root, since it is the more expensive numerical operation.

7. References

Chorin, A. (1977). Random Choise Solutions of Hyperbolic Systems. *Journal of Computational Physics*, Vol. 22, pp. 517-272, ISSN 0021-9991.

Godunov, S. (1959). A Finite Difference Method for the computation of Discontinuous Solutions of the Equations of Fluid Dynamics. *Mat. Sb.*, Vol. 47, pp. 357-393 (In Russian).

Leveque, R. (2004). *Finite Volume Methods for Hyperbolic Problems* (Second Edition), Cambridge University Press, ISBN 0-521-00924-3, Cambridge.

Toro, E., Spruse, M. and Speares, W. (1994). Restoration of the Contact Surface in the HLL-Riemann solver. *Shock Waves*, Vol. 4, pp. 25-34, ISSN 0938-1287.

Toro, E. (2009). *Riemann Solvers and Numerical Methods for Fluid Mechanics. A practical introduction* (Third Edition), Springer-Verlag, ISBN 978-3-540-25202-3, Berlin.

van Leer, B. (1985). On the Relation Between the Upwind-Differencing Schemes of Godunov, Enguist-Osher and Roe. *SIAM Journal of Scientific Computing*, Vol. 5, No. 1, pp. 1-20, ISSN 1064-8275.

Yee, H. (1989) *A Class of High Resolution Explicit and Implicit Shock-Capturing Methods*. NASA Technical memorandum 101088. Ames Research Center, California.

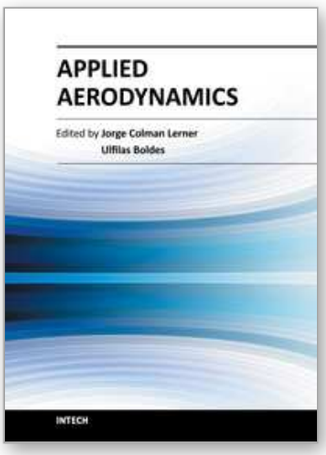

Applied Aerodynamics

Edited by Dr. Jorge Colman Lerner

ISBN 978-953-51-0611-1

Hard cover, 192 pages

Publisher InTech

Published online 11, May, 2012

Published in print edition May, 2012

Aerodynamics, from a modern point of view, is a branch of physics that study physical laws and their applications, regarding the displacement of a body into a fluid, such concept could be applied to any body moving in a fluid at rest or any fluid moving around a body at rest. This Book covers a small part of the numerous cases of stationary and non stationary aerodynamics; wave generation and propagation; wind energy; flow control techniques and, also, sports aerodynamics. It's not an undergraduate text but is thought to be useful for those teachers and/or researchers which work in the several branches of applied aerodynamics and/or applied fluid dynamics, from experiments procedures to computational methods.

InTech Europe
University Campus STeP Ri
Slavka Krautzeka 83/A
51000 Rijeka, Croatia
Phone: +385 (51) 770 447
Fax: +385 (51) 686 166
www.intechopen.com

InTech China
Unit 405, Office Block, Hotel Equatorial Shanghai
No.65, Yan An Road (West), Shanghai, 200040, China
中国上海市延安西路65号上海国际贵都大饭店办公楼405单元
Phone: +86-21-62489820
Fax: +86-21-62489821

IntechOpen